Quantitative Analyses of Precession Diffraction Data for a Large Cell Oxide

Christopher S. Own,* Arun K. Subramanian, and Laurence D. Marks

Department of Materials Science, Northwestern University, 2220 N. Campus Dr., Cook 2036, Evanston, IL 60201, USA

Abstract: Kinematical and two-beam calculations have been conducted and are compared to experimental precession data for the large unit cell crystal $La_4Cu_3MoO_{12}$. Precession electron diffraction intensities are found to exhibit approximate two-beam behavior and demonstrate clear advantages over conventional SADP intensities for use in structure solution.

Key words: TEM, electron, precession, diffraction, direct methods

INTRODUCTION

In 1986, Vincent and Bird used focused large-angle convergent beam electron diffraction zone axis patterns to obtain pseudo-kinematical intensities for use in structure refinements. These experiments stem from earlier work by Vincent et al. (1984), who used hollow-cone illumination on the zone axis to acquire the same type of data from high-order Laue zone (HOLZ) reflections. The success (and difficulties) of these experiments prompted Vincent, with P.A. Midgley, to develop a technique that uses coil deflections to sequentially sweep the beam in a conical manner through successive Bragg reflections to probe first-order reflections, which have reduced coupling due to their off-zone diffraction geometry. This is called precession electron diffraction by virtue of the conical deflection arrangement (Vincent & Midgley, 1994). Analyses to date suggest that precession pattern intensities are far less sensitive to thickness than conventional electron diffraction patterns and, if an accurate model can be derived, will simplify structure solution. In addition, experiments have uncovered a number of hidden bonuses provided by the technique, some of which are outlined in this article.

The geometry of precession electron diffraction is shown in Figure 1. The beam is rocked in a conical fashion with a wide symmetrical tilt above the specimen. After interaction with the specimen, the transmitted and diffracted beams are descanned by the projector lens deflectors to re-form a point pattern. This geometry yields several very interesting features:

- The pattern may be indexed as a conventional diffraction pattern although the intensities have actually been gathered from off-zone reflection conditions.
- Nonsystematic dynamical effects such as Kikuchi lines and intensity variations in CBED spots are reduced by averaging over incident beam directions.
- Because the beam is entering the sample from an off-axis direction, much of the dynamical scattering that is particularly strong at the exact Bragg condition (or zone axis channeling condition) is avoided.
- Many more FOLZ reflections are illuminated, under more kinematical conditions, by the Ewald sphere, allowing the acquisition of an increased number of intensities for use in structure solution techniques.
- HOLZ reflections are illuminated, yielding expanded three-dimensional data sets provided that spots from separate Laue zones do not overlap.

Figure 2a,b demonstrates these characteristics in the diffraction pattern from a thick $Mg_3V_2O_8$ crystal. A very moderate precession angle ($\sim$5 mrad) was used to form this pattern. The extension by precession of the HOLZ ring into an annulus of width 10 mrad is clearly seen, as well as blending of nonsystematic dynamical effects into a radially diffuse background. This dynamical background averaging can improve intensity measurements by considerably simplifying the problem of background subtraction.

Gemmi (2001) maintains that two-beam dynamical corrections can be made to the kinematically expected intensities if necessary and the results of a two-beam correction using the Blackman formula (Blackman, 1939) are valid in the case of electron precession. This assertion was originally postulated by Vincent and Midgley in their first
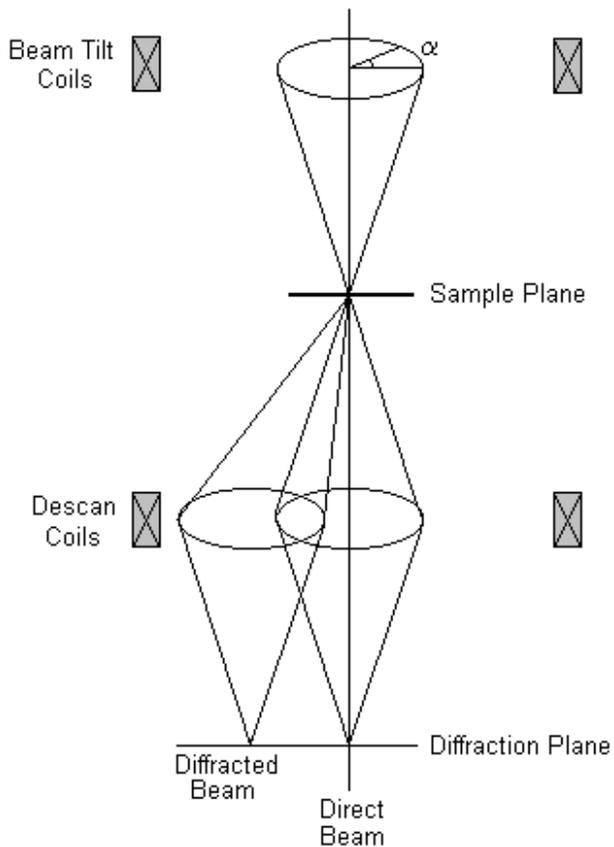
Figure 1. Precession electron diffraction geometry.

paper on precession. Gjønnes in 1997 made a comprehensive analysis of the precession diffraction geometry and proposed geometrical correction factors for the two-beam model to account for the excitation error. She also calculated the geometrical factor due to beam convergence and warned that the primary errors in precession patterns are still dynamical in nature. In this article, we investigate the validity of the two-beam model for precession by studying patterns acquired from a novel cuprate in a precession-capable Hitachi UHV H-9000 TEM and comparing them to nonprecessed diffraction data gathered from the same region of the specimen.

EXPERIMENTAL

The original paper of Vincent and Midgley described the use of a convergent beam to obtain nonoverlapping precessed CBED patterns. The intensities were acquired by using a line scan procedure similar to that used for conventional CBED analysis, where integrated line intensity was converted into integrated area using a least squares method (Berg et al., 1998). Use of CBED allows a very small probe size provided that the instrument can very accurately precess the beam about a specific region of the sample.
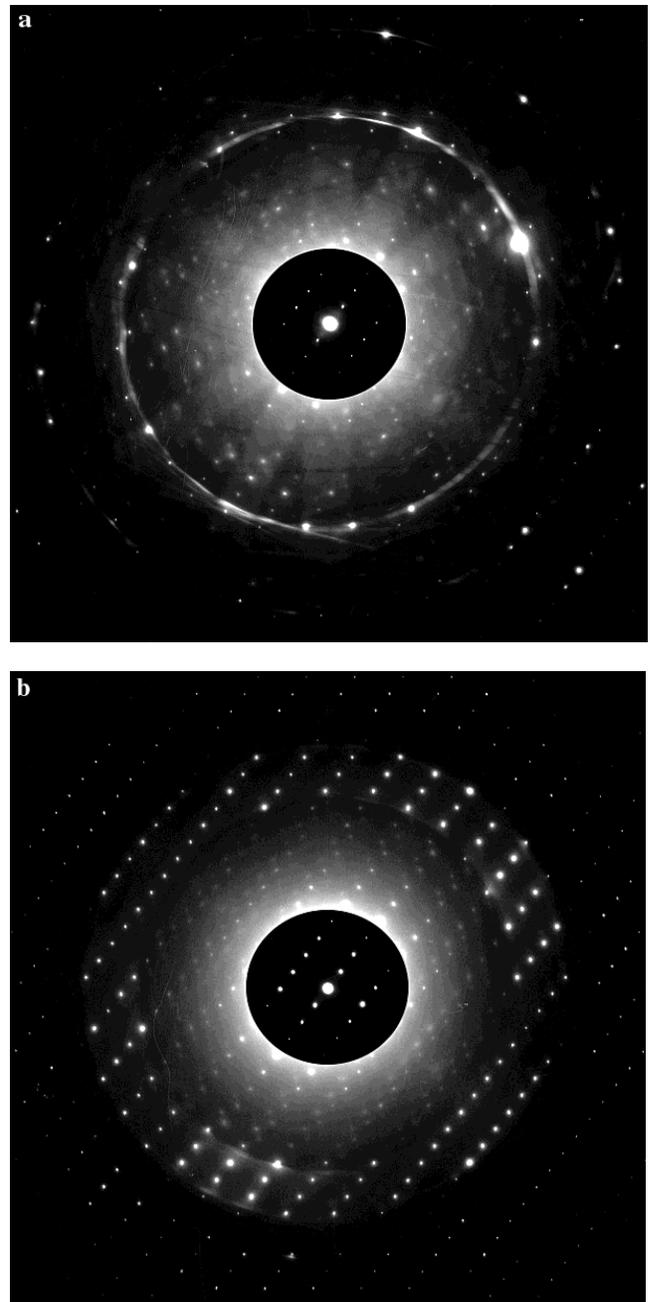

Figure 2. a: Selected area DP of the [5$\bar{3}$2] zone axis of $Mg_3V_2O_8$. **b**: Precessed SADP of $Mg_3V_2O_8$ using a moderate precession angle of 5.2 mrad. Several HOLZ annuli are apparent and nonsystematic effects in the ZOLZ are averaged into a radially diminishing background.. (Note: Images **a** and **b** have identical exposure times and digitizing conditions and have received the same digital image processing, so they can be directly compared.)

However, convergence is not strictly necessary in electron precession, and can be considered a hindrance because some specimens are susceptible to radiation damage from a focused probe and some instruments may have difficulty maintaining a pivot point at a precise area on the specimen due to condenser and objective prefield aberrations.
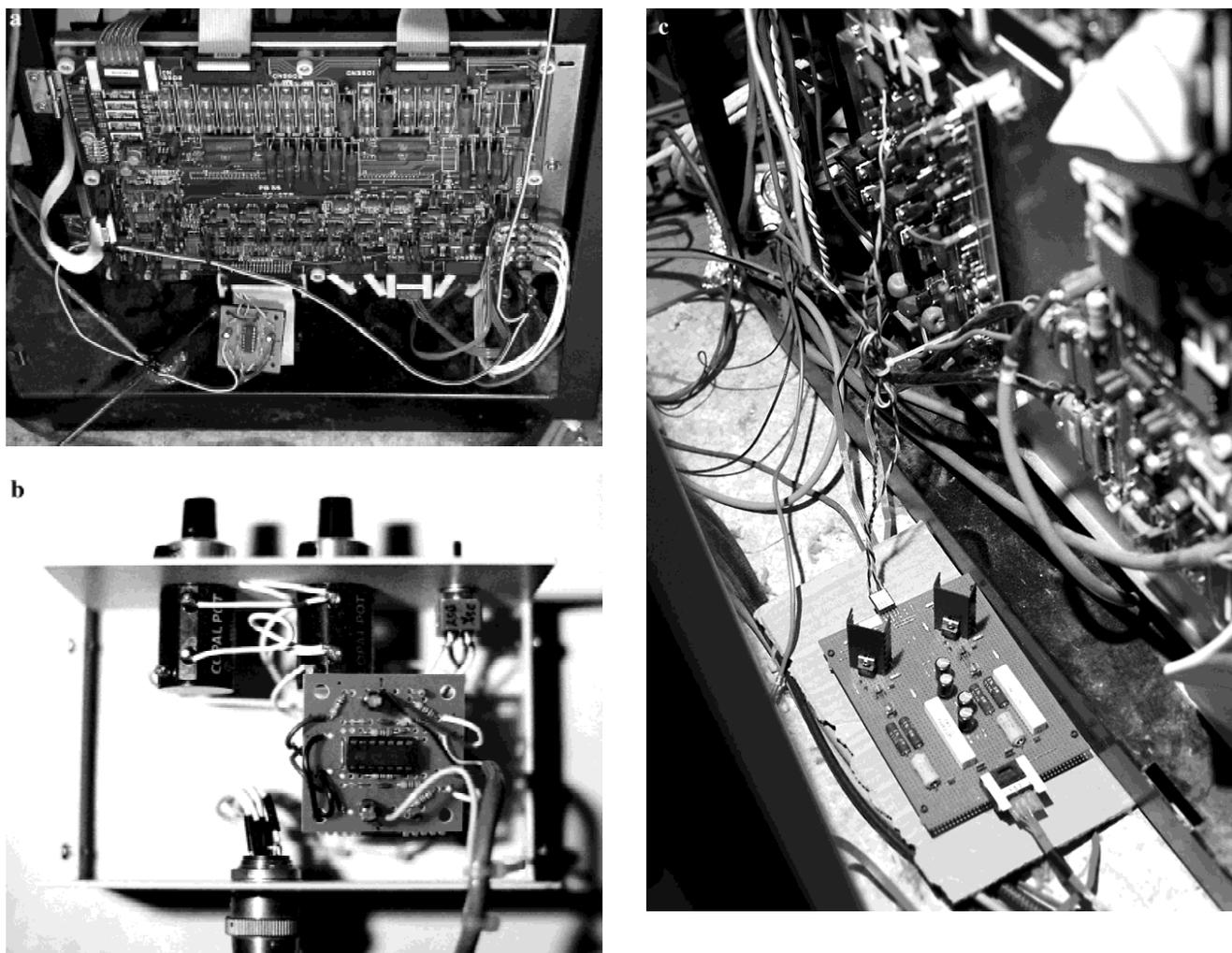
Figure 3. a, **b**: Buffered inverting mixer for tilt and descan. **c**: Descan amplifier.

Due to the limitations inherent to CBED precession, as well as practical considerations during implementation, we use a selected area precession mode with near-parallel illumination to gather sharply defined precessed spots. This allows collection of data from specific areas of the specimen, ease in aligning precession geometry (by virtue of sharp diffraction points), and loose constraints on the image plane alignment capabilities of the instrument such that precession mode can be retrofitted onto almost any existing TEM. The real-space sampling resolution in this mode of operation is limited by SA aperture size and by SA errors. (To avoid confusion, conventional SAD patterns will be referred to in this article as SADPs, whereas precession data will be henceforth referred to as "precessed," with the SA mode used to form sharp spots implicit.)

The precession hardware is a data acquisition and control (DAQ) system built around a National Instruments data control board. New electronics were designed to insert a clean external control signal generated by the PCI card.

Great attention was given to preservation of full microscope functionality such that routine instrument alignment and everyday operation were not affected in any way. The H-9000 beam deflection amplifiers were not designed to handle rapid AC signals and, as such, were redesigned and replaced with high-bandwidth amplifiers (Fig. 3). The system can output 1 MS/s per channel, resulting in a scan/descan system that operates distortion-free beyond 2 kHz before noticeable attenuation, and routinely demonstrates a scanned/descanned spot resolution of less than 0.5 mrad in the diffraction plane. It is typically operated with an angular resolution of 1° (360 subdivisions per cycle) at 60 Hz with input deflections of a few volts, translating to no more than about 800 mA of current per deflection coil. Software was written in Labview visual language and offers an infinitely configurable, user-friendly interface that includes compensations for aberration symmetries up to threefold (Fig. 4).

The software is written for real-time signal update, permitting a dynamic alignment procedure for quick distor-

tion correction. In the current software revision, modifications of the control signal can be applied during alignment through a visual minimization procedure to bring precessed reflections down to sharply focused spots. Consequently, precession alignment including distortion correction can be conducted rather painlessly within 10 min. A more detailed description of the system and its implementation will be given elsewhere (C.S. Own, submitted).

Diffraction patterns along the [001] zone axis of a $La_4Cu_3MoO_{12}$ crystal were taken in both selected area and precession modes (~20 mrad precession angle). Nine negatives comprised each exposure series and were digitized using an Optronics microdensitometer at a scale of 25 μm per pixel. SADP intensities were then acquired by pattern matching a unitary spot motif to the digitized diffraction spots and then integrating the intensity of the matched pattern. Precession intensities were quantified in a slightly different way by first applying a background subtraction algorithm within a masked area around each spot and then integrating the remaining intensity.

Reduction of nine data sets into a single set was conducted by scaling the data from each negative while minimizing the overall error between data sets. Details of this procedure can be found in a previous paper from our group (Xu et al., 1994). Intensities from the precession exposure series matched very well when scaled, resulting in extremely low error between negatives. Compared to the conventional SAD data set, the precession data set had errors at least an order of magnitude better. This is an important practical point, and can be attributed to the fact that the precession technique is much less sensitive to minor variations in the experimental conditions and is consequently less susceptible to systematic errors than the SAD methods. Precession provides nearly the same intensities for symmetry-equivalent reflections and is fairly tolerant of a slightly off-zone diffraction condition.

Results and Discussion

$La_4Cu_3MoO_{12}$ is a complex oxide exhibiting "frustrated" magnetic behavior. The structure is a homeotype of $YAlO_3$, a rare-earth hexagonal phase. The crystal is very slightly monoclinic but was assumed to have a rectangular cell for the calculations. Unit cell parameters are $a = 6.86$ Å, $b = 10.98$ Å, and $c = 7.9147$ Å, and $\beta = 90.02°$ (Vander Griend et al., 1999). The structure is shown in Figure 5. Intratriangle antiferromagnetic interactions align two of three spins, yielding trimers with $S_{total} = \frac{1}{2}$. This spin coupling causes an ordering between adjacent cells that doubles the unit cell along the a direction.

Figure 6a–c shows the diffraction patterns for calculated, SADP, and precessed reduced diffraction data sets (non-symmetry-averaged). The intensity of each reflection is represented using gray scale as well as spot size to visually demonstrate relative spot intensities. (040)-type reflections in the kinematical pattern are considerably more intense than other reflections in the pattern. This high intensity is not apparent in the SADP pattern nor in the precessed pattern. Clearly, dynamical interaction cannot be avoided near the transmitted beam, even with precession. However, the fine details in the diffraction map are rather well preserved in the precessed DP. With precession, the variation in intensity between adjacent reflections is clearly displayed, and the alternating spots show, qualitatively, appropriate ratios. The SAD pattern, in contrast, loses some fine infor-
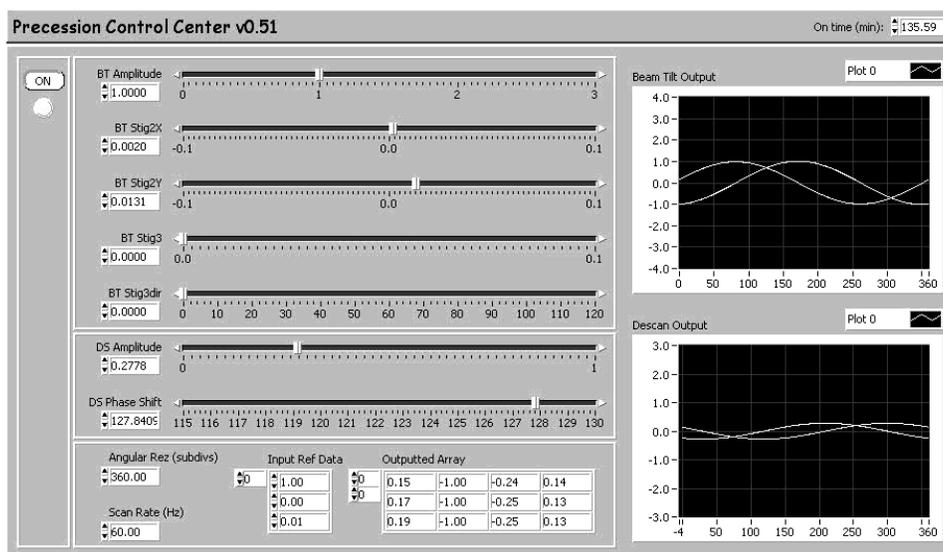

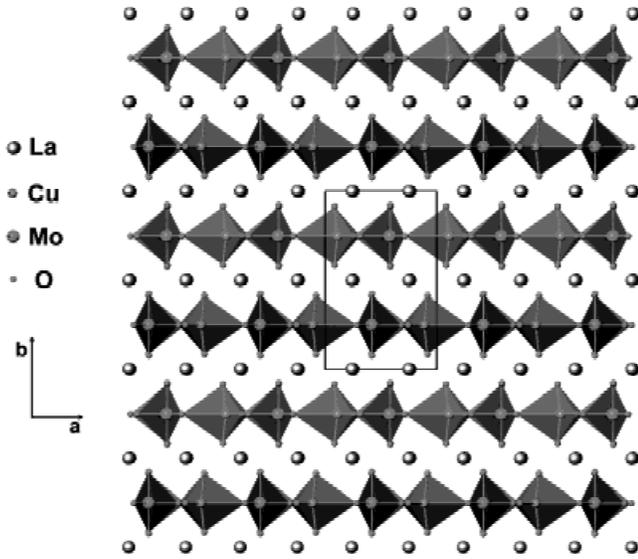**Figure 4.** Version 0.51 of the precession control software.

Figure 5. [001] zone axis of La$_4$Cu$_3$MoO$_{12}$.

mation such as the subtle intensity ordering in the reflections that occur between the (230) and (2$\bar{3}$0) spots.

To better quantify the relationship between precessed and nonprecessed patterns, a Blackman curve was calculated for a crystal thickness of 50 nm using the two-beam equation

$$\frac{I_{2\text{-}beam}}{I_{kin}} \propto \frac{1}{A_{hkl}} \int_0^{A_{hkl}} J_0(2x)\, dx \qquad (1)$$

where the integration limit $A_{hkl} = 2\pi e m_0 t V_g / h^2$. Electron scattering factors were computed from values provided with the NCEMSS multislice software (Kilaas, 2003), and experimental isotropic Debye-Waller factors acquired from X-ray data were included in the calculation of the lattice potential. This ratio is directly comparable to the nonprecessed diffraction intensity (I_{SADP}) divided by the calculated kinematical intensity. The precessed intensity, however, cannot be directly compared to the Blackman calculation because it is integrated over angle α (see Fig. 1) rather than excitation error. Intensities measured from precession patterns must be converted using the relationship

$$I_{prec} \propto g \sqrt{1 - \left(\frac{g}{2R_0}\right)^2} \cdot \int_0^{2\pi} I_g(\alpha)\, d\alpha. \qquad (2)$$

The geometrical prefactor accounts for excitation error only; an extra factor of $1/g \cdot \sqrt{1 - (g/2R_0)^2}$, suggested by Gjønnes for beam convergence, has been omitted, because the precession patterns were acquired using parallel illumination. R_0 is the radius of the zeroth-order Laue zone, calculated to be 1.015 Å^{-1} for this experiment. The results are plotted in Figure 7, wherein the y-axis represents the ratio of calcu-

lated as well as measured dynamical-to-kinematical intensity ratios and is unitless.

Comparing two-beam theory (dots) to the precession data (circles), the intensity ratios cluster along the curve but do not appear to exactly follow two-beam theory. At higher (>3) A_{hkl} values, intensity ratios are too low. However, the general trend of the precession data is distinctively Blackman-like in the critical region before the first oscillation of the Bessel integral: Intensity ratios decrease with increasing A_{hkl}. Compared to the nonprecessed SADP intensities (triangles), the precessed data exhibits behavior far closer to two-beam theory than SA diffraction. Figure 7 does not show all SAD data points collected in the current x-axis range. Roughly 50 data points reside above the maximum intensity ratio scale shown on the plot and are distributed over various A_{hkl}. The precession data also contains about half a dozen outliers at very low A_{hkl} that are several orders of magnitude too large (not shown). However, these occur only for $A_{hkl} < 0.1$—caused by division by very small kinematical intensities—and do not express the apparently random scatter of SADP intensity ratios.

The above result is not sufficient to dismiss two-beam theory as a good model of precession intensity behavior. Given the clustering behavior of the precession outliers at small A_{hkl}, the deviations from the two-beam calculation are likely due to two related sources of error:

1. The experimental diffraction patterns for the [001] zone were found to be slightly different from the expected structure proposed by Vander Griend et al. (1999). In the calculated kinematical pattern, $h =$ odd reflections manifest as extremely dim spots in between columns of strong reflections. In the experimental patterns, they were absent, indicating that the crystal under study was likely a different phase from that which was expected. The presence of the strong $h =$ even reflections and preservation of the expected symmetry in experimental patterns indicates that the overall lanthanum framework structure is identical. However, loss of odd-h reflections in experimental patterns signifies a relaxation of the magnetically frustrated structure and, hence, a very slight change in the arrangement of metal-oxygen tetrahedra within the La framework. This will cause a modification of structure factors, with the largest errors corresponding to small structure factors that represent small scattering contributions.

2. For La$_4$Cu$_3$MoO$_{12}$, the majority of structure factors correspond to large A_{hkl}. Unfortunately, with increasing A_{hkl}, the two-beam approximation begins to break down. Low intensity generally corresponds to small structure factor, which corresponds to low A_{hkl}. This means that for this crystal, few low A_{hkl} reflections exist that can strongly demonstrate the Blackman trend, rendering it difficult to precisely map out the behavior in the region of A_{hkl} where two-beam behavior is most dominant (very high angle reflections and/or reflections with low structure fac-
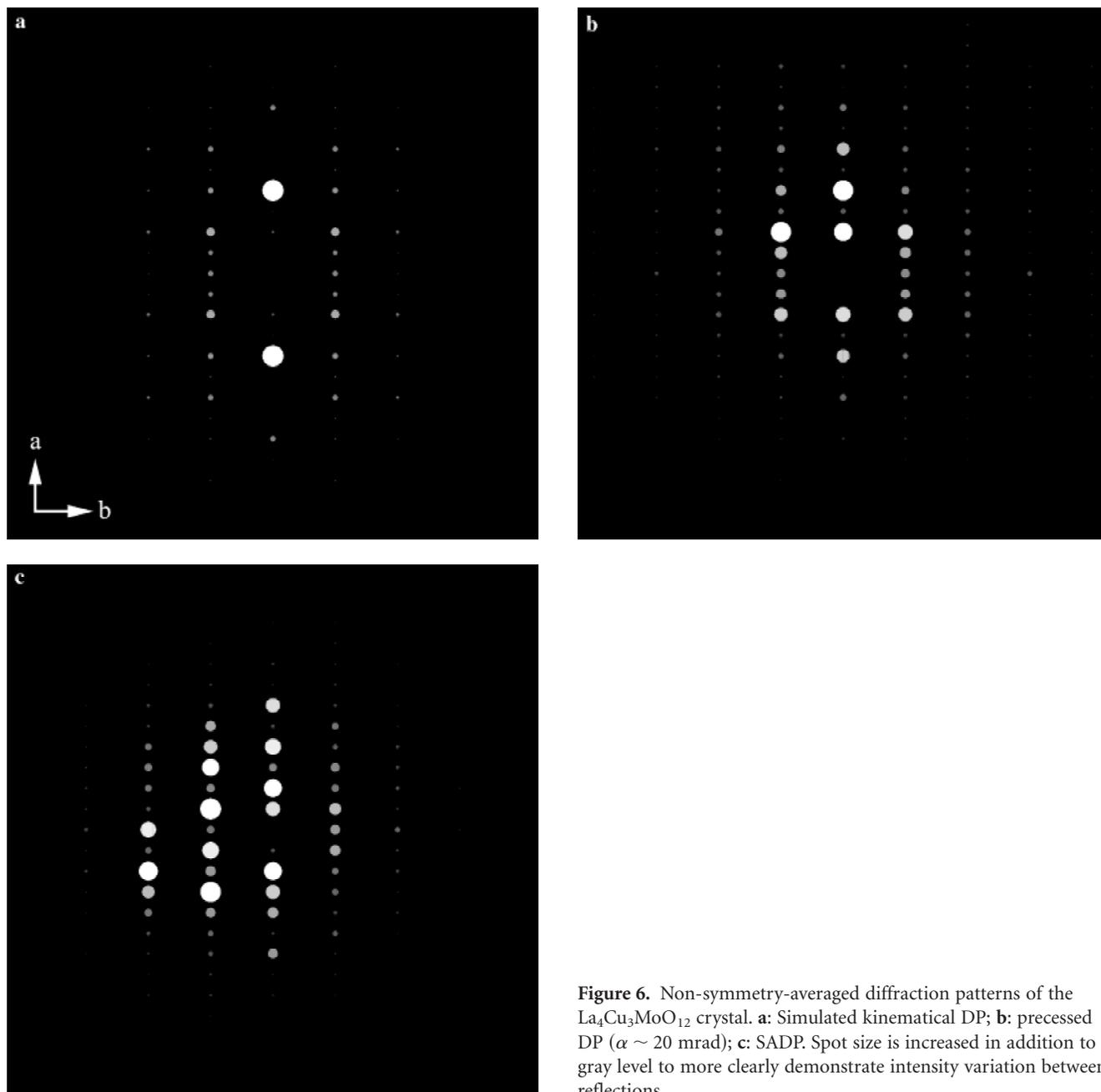
Figure 6. Non-symmetry-averaged diffraction patterns of the $La_4Cu_3MoO_{12}$ crystal. **a**: Simulated kinematical DP; **b**: precessed DP ($\alpha \sim 20$ mrad); **c**: SADP. Spot size is increased in addition to gray level to more clearly demonstrate intensity variation between reflections.

tor). It is likely that the missing $h =$ odd reflections represent data points that would more clearly show the intensity behavior in the region of the Blackman plateau.

While not definitively two-beam in nature, precession pattern intensities are nevertheless superior to conventional diffraction intensities. To demonstrate the quality of the precessed intensities, a simple experiment was carried out by combining phase information from the known crystal structure with symmetry-averaged experimental intensities. The real-space potential maps of the [001] zone are shown in Figure 8a–c. Refer to Figure 5 for atom locations from the known structure.

It is well known that the phase contains the dominant information in the structure; Fourier inversion will generate potentials that closely resemble the structure from which the phase was extracted. Nevertheless, the potential maps demonstrate subtle but striking differences between precession and SA diffraction intensities. The precession-derived map (Fig. 8b) exhibits sharp, contrasty features clearly delineating likely atom positions and potential wells, whereas the SADP-derived potential (Fig. 8c) is much fuzzier. Neither of
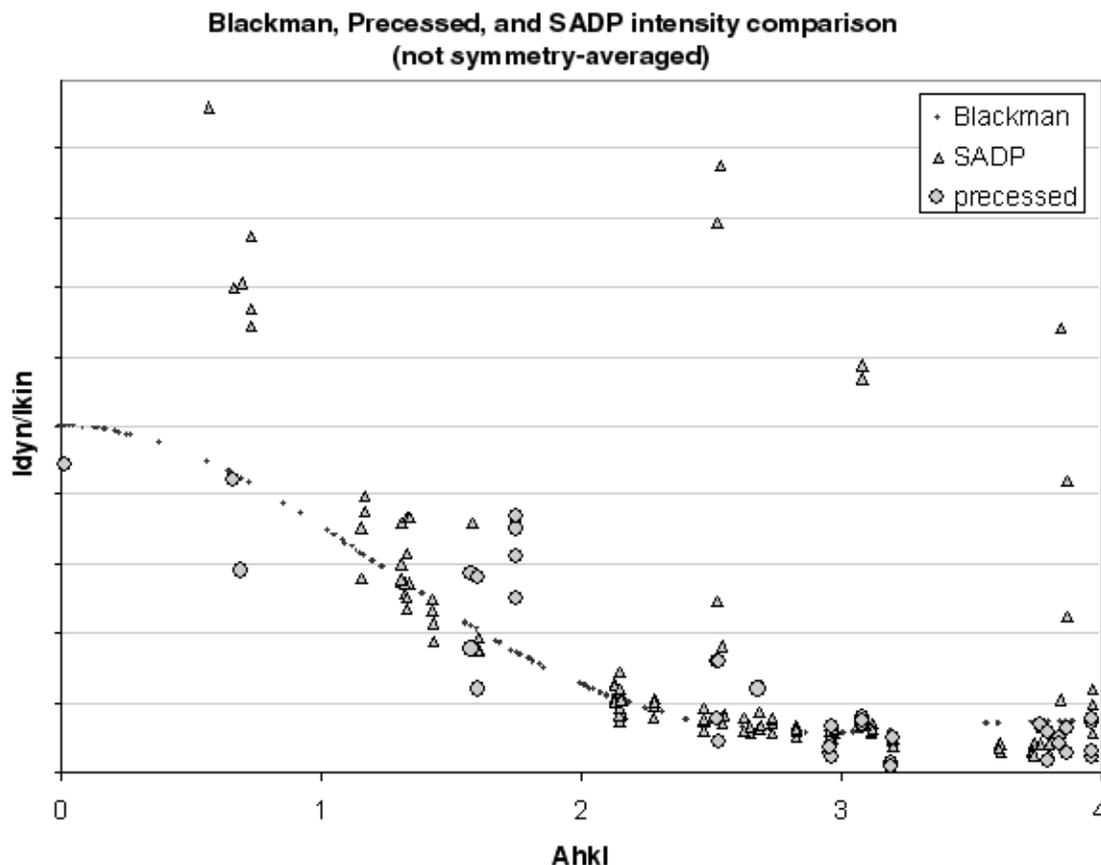
Figure 7. Measured and calculated intensity ratio between dynamical and kinematical intensities. The experimental data is normalized to match the calculated Blackman curve, which plateaus at $I_{dyn}/I_{kin} = 1$ (y-axis plotted linearly).

the experimentally derived images unambiguously pinpoints the weakly scattering oxygen atoms arranged around each lanthanum atom. However, upon closer inspection, one can see that the structure from SADP intensities contains medium potential artifacts where O atoms simply do not exist, whereas the precession-derived map more clearly pinpoints these weak scatterers.

Conclusion

The assertion that two-beam theory can exactly predict precession intensities does not appear to be completely accurate because the precessed data set does not closely follow the Blackman curve at low A_{hkl}. This result would become more compelling if more high-angle reflection intensities were sampled or if the two-beam calculation was performed on the true crystal structure rather than the expected one. The next logical step is to apply modern direct methods techniques to the intensity data to determine a structure that could then be used for a more accurate theoretical two-beam calculation by virtue of more correct structure factors. Discovery of a different phase

warrants an investigation of the new structure and its magnetic behavior, which may yield information on how cation arrangement affects magnetic properties, a primary focus in the development of new high-temperature superconductors.

Whether or not the two-beam model is accurate, precession data still demonstrate clear advantages over nonprecessed patterns, and behave much more like the two-beam prediction than nonprecessed DPs. The experiments show that the technique will undoubtedly provide considerably enhanced intensity data for use in structure solution.

At the time of this writing, to our knowledge, there are four instruments in the world that are precession capable. Given the apparent advantages of precession, more precession-enabled instruments are sure to surface in the coming years. The do-it-yourself DAQ approach proves to be very flexible and extremely inexpensive; instrumentation costs for the Northwestern University system totaled under US$2000. This is a rather small cost for any high-end characterization system. With suitable beam-deflection systems already inside many STEM and tomography systems, the cost of modification and/or retrofit into existing systems will be further diminished.
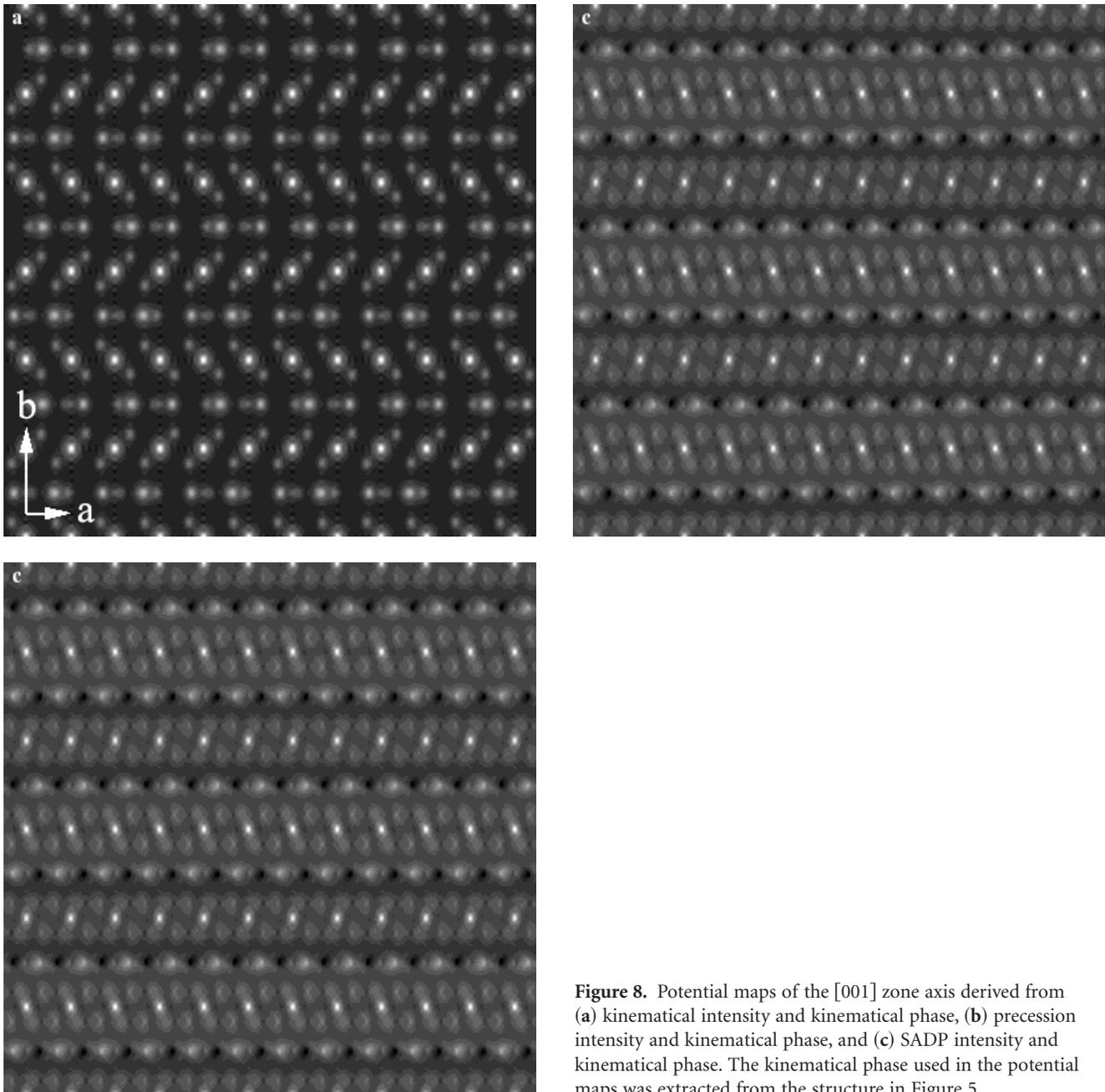
Figure 8. Potential maps of the [001] zone axis derived from (**a**) kinematical intensity and kinematical phase, (**b**) precession intensity and kinematical phase, and (**c**) SADP intensity and kinematical phase. The kinematical phase used in the potential maps was extracted from the structure in Figure 5.

ACKNOWLEDGMENTS

REFERENCES

BERG, B.S., HANSEN, V., MIDGLEY, P.A. & GJØNNES, J. (1998). Measurement of three-dimensional intensity data in electron diffraction by the precession technique. *Ultramicroscopy* **74**, 147–157.

BLACKMAN, M. (1939). On the intensities of electron diffraction rings. *Proc Roy Soc A* **173**, 68–82.

GEMMI, M. (2001). Precession technique. In *Electron Crystallography and Cryo-Electron Microscopy*, Puiggali, J., Rodriguez-Galan, A., Franco, L. & Casas, M.T. (Eds.), pp. L91–L94. Barcelona: Barcelona Universitat Politecnica de Catalunya.

GJØNNES, K. (1997). On the integration of electron diffraction intensities in the Vincent-Midgley precession technique. *Ultramicroscopy* **69**, 1–11.

KILAAS, R. (2003). *NCEM Software Resource*. Retrieved 01 January, 2003 from http://ncem.lbl.gov/frames/software.htm.

VANDER GRIEND, D.A., BOUDIN, S., CAIGNAERT, V., POEPPELMEIER, K.R., WANG, Y.G., DRAVID, V.P., AZUMA, M., TAKANO, M., HU, Z.B. & JORGENSEN, J.D. (1999). $La_4Cu_3MoO_{12}$: A novel cuprate with unusual magnetism. *J Am Chem Soc* **121**, 4787.

VINCENT, R. & BIRD, D.M. (1986). Measurement of kinematic intensities from large-angle electron-diffraction patterns. *Phil Mag Lett* **53**, L35–L40.

VINCENT, R., BIRD, D.M. & STEEDS, J.W. (1984). Structure of AuGeAs determined by convergent-beam electron-diffraction. 2. Refinement of structural parameters. *Phil Mag A* **50**, 765–786.

VINCENT, R. & MIDGLEY, P.A. (1994). Double conical beam-rocking system for measurement of integrated electron-diffraction intensities. *Ultramicroscopy* **53**, 271–282.

XU, P., JAYARAM, G. & MARKS, L.D. (1994). Cross-correlation method for intensity measurement of transmission. *Ultramicroscopy* **53**, 15–18.